Available online at www.sciencedirect.com

SciVerse ScienceDirect

Ceramics International 39 (2013) 1315–1325

CERAMICS INTERNATIONAL

www.elsevier.com/locate/ceramint

Strombus gigas inspired biomimetic ceramic composites via SHELL—Sequential Hierarchical Engineered Layer Lamination

Gregory Karambelas[a], Sridhar Santhanam[a,*], Zachary N. Wing[b]

[a]Mechanical Engineering Department, Villanova University, Villanova, PA 19085, United States
[b]Advanced Ceramics Manufacturing, Tucson, AZ 85756, United States

Received 24 May 2012; received in revised form 20 July 2012; accepted 20 July 2012
Available online 26 July 2012

Abstract

Nature has produced remarkable structural designs based on many millennia of evolutionary optimization. Biological materials, such as the sea-shell, possess unique microstructures and properties that provide inspiration for the next generation of structural ceramics. Strombus gigas (Queen conch) shells contain a hierarchical, multilayered, crossed-lamellar architecture built with two natural materials (calcium carbonate and protein) with at least three identifiable scales (or orders) of structure. Drawing on Strombus gigas for inspiration, we have developed a new process to realize such complex micro-architectures in macroscopic form. SHELL (Sequential Hierarchical Engineered Layer Lamination) is a thermoplastic forming process that is capable of producing the third order structural complexity over the micron-millimeter length scales. We have fabricated silicon nitride—boron nitride ceramics via SHELL that are endowed with excellent damage tolerance, exhibit graceful failure, and exhibit toughening mechanisms similar to those observed in Strombus gigas.

Keywords: A. Extrusion; C. Toughness and toughening; D. Nitrides

1. Background

Bioinspired structural materials have attracted a lot of attention as materials scientists seek to draw inspiration from biological organisms [1]. Biological materials usually have a very complex hierarchical architecture and are also strongly multifunctional. These materials are made by self-assembly and possess special capabilities such as self healing [2,3]. Natural hard and tough materials, like Mollusc shells, have been a subject of intense study both by biologists and materials scientists. These shells possess a unique combination of mechanical properties including high elastic modulus, strength, and toughness [4,5]. Mollusc shells come in several different forms: nacreous, foliated, prismatic, crossed-lamellar, and homogeneous. Of these, the nacreous form has been the most studied [5–9] with its 'brick and mortar' architecture the easiest to emulate. The crossed lamellar architecture, seen in the Strombus gigas (Queen conch), has also been the subject of extensive study [10–12]. In comparison to nacreous shells, this architecture is far more complex.

The Strombus gigas shell has evolved to optimize tolerance to damage caused by projectile rocks and debris from waves and also from predator attacks. It does this through fracture energy dissipation throughout the shell as it experiences the impact force. The microstructure of the Queen conch shell can be seen in Figs. 1 and 2. The shell consists of three major macroscopic layers: inner, middle, and outer (see Fig. 1). Each of the major layers is composed of long parallel laths or first order lamellae. While the inner and outer layers have the first order lamellae (laths) with the same orientation (0°), the middle layer's first order lamellae are oriented perpendicular (90°) to those of the inner and outer layers. In the middle layer, each first order lamella is composed of the second order

*Corresponding author. Tel.: +1 610 519 7924; fax: +1 610 519 7312.
E-mail address: sridhar.santhanam@villanova.edu (S. Santhanam).

0272-8842/$ - see front matter © 2012 Elsevier Ltd and Techna Group S.r.l. All rights reserved.
http://dx.doi.org/10.1016/j.ceramint.2012.07.067

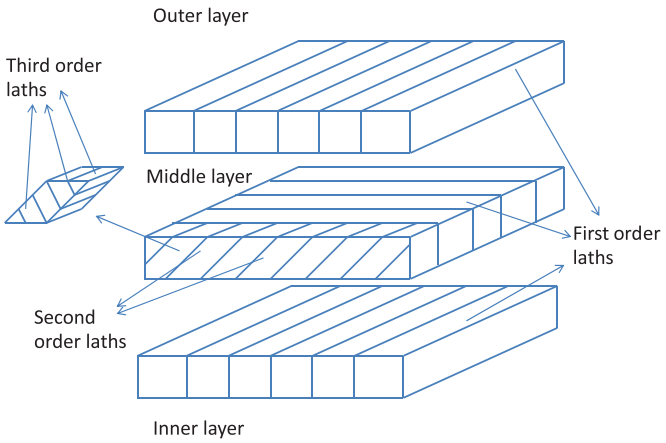

Fig. 1. The crossed lamellar microstructure of the Strombus gigas: a schematic adapted from [13].

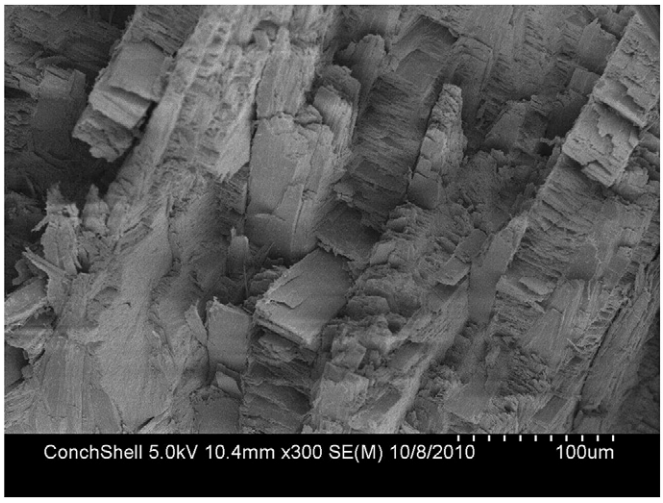

Fig. 2. The crossed lamellar microstructure of the Strombus gigas shell: scanning Electron Micrograph. The first and second order lamellae are visible on this fracture surface.

lamellae which are parallel laths whose long axes are oriented at approximately 45° to the long axis of its first order lamella. Also, the second order laths in two adjacent first order lamellae have perpendicular orientations. Each second order lamella in turn is composed of parallel third-order laths (Fig. 1). The scale of these layers ranges from 100 nm to about 60 μm [14].

All interfaces in this rich micro-architecture are filled with an organic matrix, which comprises less than 1 vol.% of the shell's structure. This matrix surrounds and separates the lamellar orders of the stiffer, stronger, and more brittle aragonite phase [14]. Damage tolerance of a Strombus gigas shell is remarkable compared to its primary component—aragonite $CaCO_3$. One measure of damage tolerance in these materials is the Work of Fracture (WOF). WOF is a measure of the work required to generate a unit area of fracture surface as a structure undergoes complete fracture. The WOF of pure aragonite is 0.6×10^{-3} kJ/m^2. However, the WOF of Strombus gigas shells has been measured at 13 kJ/m^2 [14]—an increase of over three orders of magnitude. The high WOF arises from at least two distinct energy absorbing mechanisms. The first is a tunnel cracking mechanism in the inner and outer layers of the shell. The second is a crack bridging mechanism that occurs as a tunnel crack penetrates into the middle layer [11].

There have been several recent attempts at replicating the intricate structure of these biological materials. Synthetic versions of nacre have been widely attempted. An early version, by Clegg et al. [15], involved the pressing and sintering of thin sheets of silicon carbide coated with graphite. The graphite coating created weak interfaces in the ceramic leading to crack deflection as the primary mechanism of toughening. A similar strategy was adopted by Mayer [16]. Alumina tablets were bonded together with adhesive tapes and resulted in a ceramic composite material system with a high toughness. Other recent innovative approaches have included ice templating [17] and layer-by-layer deposition [18].

Fabrication of synthetic versions of the crossed lamellar structure has been explored on a limited scale. Chen et al. [19] used MEMS (micro-electro-mechanical systems) processing methods to fabricate a crossed-lamellar structure using polysilicon and photoresist. Kaul and Faber [20] utilized a process combining templated grain growth, tape casting, and oriented lamination to form a second order crossed lamellar structure in mullite. In these studies, the structures developed were primarily second order. Also, the processed ceramics were not characterized from the standpoint of mechanical properties.

A non-biomimetic approach to fabricating damage tolerant ceramics has led to the development of a class of ceramics called Fibrous Monoliths (FMs). In general, Fibrous Monolith (FM) ceramics achieve damage tolerance by incorporation of weak interfaces to promote crack deflection and delamination [21]. Halloran et al. [22–24] developed the method further with a co-extrusion process to produce FM materials. The most characterized FM system is the Si_3N_4-BN Fibrous Monolith. The WOF in Si_3N_4-BN Fibrous Monoliths was significant compared to that of bulk Si_3N_4. It has been reported that the WOF for Si_3N_4 is 0.160 kJ/m^2 and that of the corresponding FM is 4.6 kJ/m^2 [23]. Comparatively, the crossed lamellar structure of the Strombus gigas produces a greater relative increase in WOF with respect to that of its basic building blocks.

To generalize, a few observations can be made on the current state-of-the-art of biomimetic or bioinspired materials based on mollusc shells. First, most fabrication efforts have focused on nacreous structures based on inorganic platelets and organic/metal interfaces. Second, although significant effort has been spent on characterizing the mechanical behavior of the crossed lamellar structure of Strombus gigas, very limited efforts have been directed toward the mimicking of their structure in engineering

materials. To be sure, replicating the feature complexity and length scales observed in these natural molluscan shells is no easy task as the body of work is almost exclusively limited to thin or microscopic samples. As noted by Launey et al. [17], achieving a practical biomimetic material in bulk form has not been possible largely due to processing difficulties.

In the present work, we demonstrate a method to create biomimetic ceramics that mimic the micro-architecture of the Strombus gigas shell and possess high damage tolerance. These ceramics will henceforth be referred to as biomimetic SG ceramics (SG for Strombus gigas). A processing method called SHELL (Sequential Hierarchical Engineered Layered Lamination) was developed to realize the first, second, and third order crossed lamellar microstructures. The process was demonstrated in a model ceramic system with silicon nitride as the bulk material and boron nitride as the interface material. The biomimetic SG ceramic materials were built up with the first order features in the millimeter scale and third order layers in the micron scale. Damage tolerance was assessed by experimentally measuring the work-of-fracture.

2. Processing

Ceramic powders blended into a thermoplastic binder enable complex green forming via shearing, compaction, extrusion, and lamination. Co-extrusion methods have been the key to producing Fibrous Monolith microstructures and provide a suitable avenue to achieve simple first order layered structures in bulk ceramics. However, co-extrusion is not capable of achieving the second or third order complexities desired in biomimetic SG ceramics. But the extrudate from a co-extrusion process can serve as the basic building block to achieve hierarchical biomimetic SG microstructures.

In this study, we utilize a process called SHELL (Sequential Hierarchical Engineered Layer Lamination) to sequentially build multiorder microstructures from macroscopic layers. Conceptually, forming the basic building block is the first step and it occurs via the sequential co-extrusion of the bulk material and the interface material. Co-extrusion provides a processing route to achieve dimensional reduction via re-extruding bundled extrudate and a route to orient particles via shear forces in the extrusion head. Using this method, we readily achieve a base material with 39 microlayers/mm (*XY* configuration, Fig. 3) that can be manipulated (through a series of cuttings and rotations) to yield the second and third order complexities.

In terms of complexity, the *XY* layer is considered to be the first order. In the layer schematic (Fig. 3), blue corresponds to Si_3N_4 and green corresponds to BN. With a single cutting and rotation operation, layer *XY* (the virgin extrusion configuration) can be reconfigured into layers *XZ* and *YZ*. Note either *XZ* or *YZ* may be considered to be comparable to the weak 'tunnel-cracking'

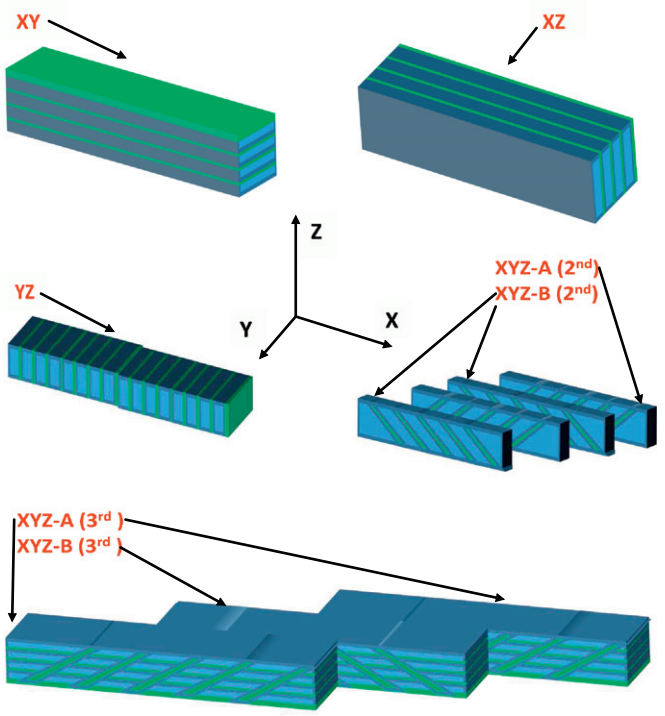

Fig. 3. Design layer configurations explored and targeted for constructing Strombus gigas based ceramics. The *XY* laminate is the foundational building block. A vertical cutting operation, performed on the *XY* laminate with the cutting plane perpendicular to *XY*, followed by rotation leads to the first order *XZ* and *YZ* configurations. An angled cutting operation (illustrated in Fig. 4) on the *XY* laminate leads to the formation of the second and third order structures *XYZ*. (For interpretation of the references to color in this figure caption, the reader is referred to the web version of this article.)

layer (outer layer in Fig. 1) observed in Strombus gigas. In the convention adopted in this paper, the *YZ* configuration is assumed to be the weak 'tunnel-cracking' layer (based on the orientation of test samples). The remaining layers in Fig. 3 are the *XYZ* second and third order layers with alternating orientations ($\pm 45^{\circ}$) for BN interfaces as one steps through the *Y*-direction. These higher order structures are produced by additional cutting and rotational steps (Fig. 4) to achieve the full three dimensional variation in interfaces. Interface angles are readily varied by changing the cutting angle. Thus, it is possible to engineer high order layers with variable geometry that can be laminated into a bulk structure.

Our ceramic composite material was based on Si_3N_4 (0.6 μm, Grade M11, H.C. Stark) and h-BN (0.7 μm, Grade NX-1, Momentive) that serve as the aragonite and interface analogues, respectively. Ceramic powders were blended into an acrylate based vehicle using a high shear mixer as described in [22].

The *XY* laminate of Fig. 3 with alternating Si_3N_4 and BN layers was formed from a master feed rod (25.4 mm × 25.4 mm square, 10% BN, Fig. 5a). Extrudate was formed using a 10:1 reduction head. Co-extrusion was performed a total of three times to produce a three-pass

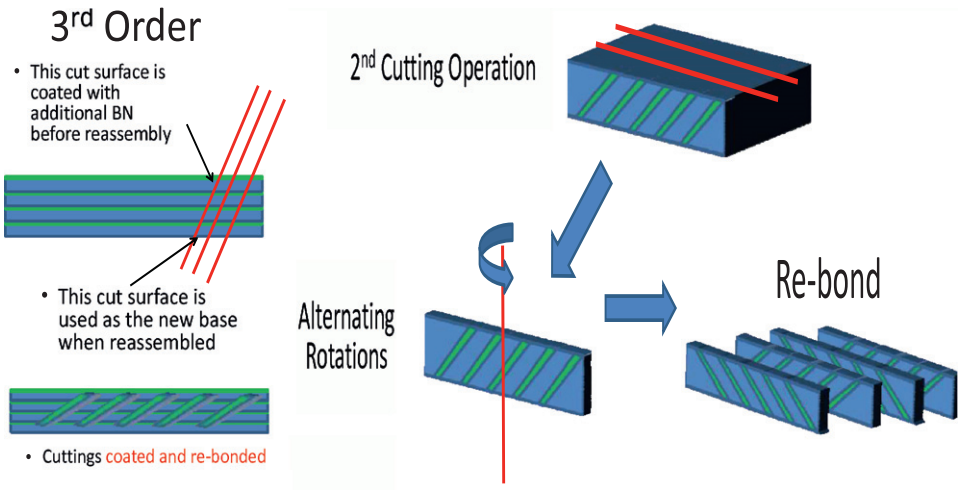

Fig. 4. An angled cutting operation on the *XY* laminate leads to the formation of the second order structures. A similar cutting operation followed by a BN coating process and reassembly leads to the third order structures. A second cutting operation performed on the second (and/or third) order laths followed by rotations and rebonding creates a layer that resembles the middle layer of the Strombus gigas shell (Fig. 1).

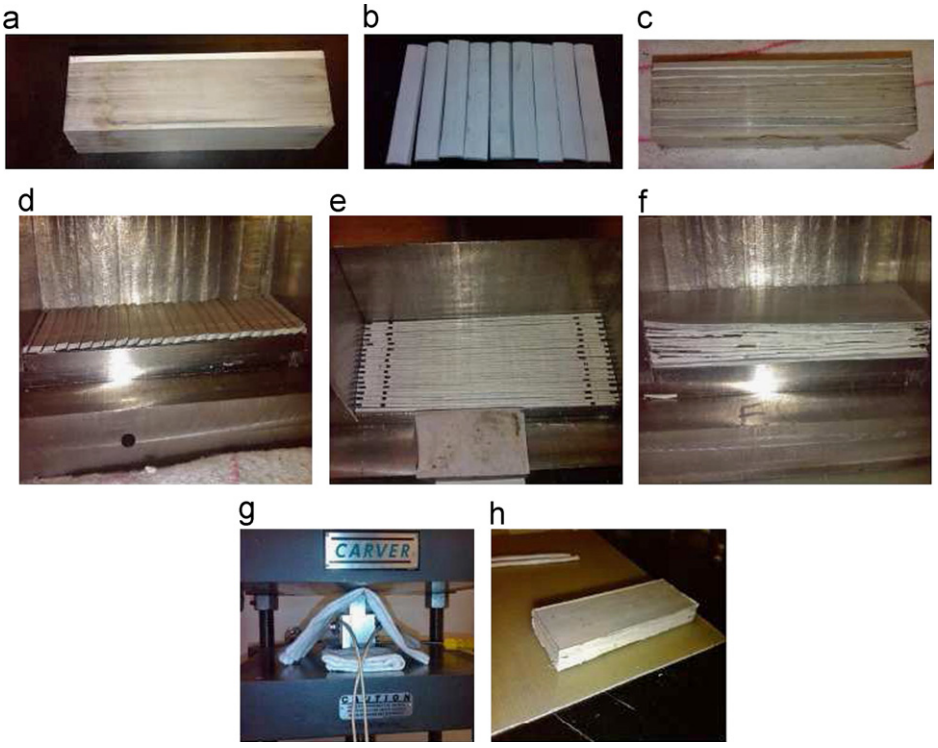

Fig. 5. Steps involved in the building of a green biomimetic ceramic. Top row: (a) first stage master feed rod, (b) co-extruded ribbons from the first extrusion pass, and (c) feed rod for the second stage. Middle row: sequence of steps for building a lamination with the second order features. Bottom row: (g) thermal lamination of build leading to, (h) the completed 'green' biomimetic build.

ribbon (i.e. a theoretical reduction of 1000× from the master feed rod size). This value was selected based in part on the number of co-extrusion passes (three) and the particle size of BN powder since it takes a minimum of several particles of BN to form a complete layer. Based on these inputs, a target of 2−3 μm was set for the BN layer thickness after the third and final co-extrusion pass. Co-extruded ribbons are shown in Fig. 5b and a stacking of ribbons that produce an intermediate stage feed rod for the co-extrusion process is shown in Fig. 5c.

The three-pass co-extrusion process was used to build up the first order *XY* laminate structure of Fig. 3. The second and third order structured layers were built up by a sequence of cutting, rotation, and rebonding steps (Figs. 4 and 5d and e) leading to the final lamination (Fig. 5f). Each layer/lamination cycle was performed using

a custom 25 mm × 75 mm steel die located within a hydraulic press (Carver Press, 7 MPa, 145 °C, Fig. 5g), thus forming the completed 'green' biomimetic build (Fig. 5h). The acrylate binder was removed in a heated nitrogen atmosphere using a 60 h 600 °C cycle. All samples were hot pressed within a uniaxial, resistively heated graphite furnace (at 1750 °C, 1 h, and 30 MPa).

3. Biomimetic design architectures

Several sample biomimetic architectural designs were conceived, fabricated, and tested. While these designs drew inspiration from the Strombus gigas shell, they were not exact replicas of the layout of Fig. 1. The architectural design layouts also reflected the fact that the physical samples fabricated were primarily meant for four point bending tests to measure the work-of-fracture. Each successive design layout was iteratively developed based on results (or lack thereof) of earlier designs. The design versions were labeled 'SG-X' (SG for a Strombus gigas inspired design and 'X' representing the design prototype iteration label). The most interesting and viable designs are shown in Figs. 6 and 7. All designs invoked the hierarchical design principle based on Strombus gigas.

The first prototype SG-A (Fig. 6a) was built with just the first order layers similar to the outer layer of the Strombus gigas shell (Fig. 1). There are three macrolayers in SG-A, with the bottom (and top) macrolayer oriented to create the phenomenon of tunnel cracking in a four-point bend test. These tunnel cracks are initiated and propagate along the many parallel, weak, thin BN layers that are oriented perpendicular to the bending tensile stress in the length direction (X in Fig. 6) of a four-point bend specimen. All three macrolayers in SG-A had only the first order structures and did not have the second and third order features seen in Figs. 1 and 2. Tunnel cracking, an important toughening mechanism seen in Strombus gigas, was observed in SG-A bend test specimens. However, strengths and work-of-fracture measures for SG-A were low. Subsequent design prototypes were conceived and fabricated based on lessons learned from SG-A. Additional features that are seen in Strombus gigas, such as the second and third order architectures, were added. Design strategies that are not seen in the Strombus gigas were also considered and included. For instance, design prototypes that included more than three macrolayers were fabricated. The tunnel cracking macrolayer was relocated to the interior of the structure rather than being the first line of defense. Some macrolayers resembled the XZ and the XY layers of Fig. 3, features that are not seen in Strombus gigas.

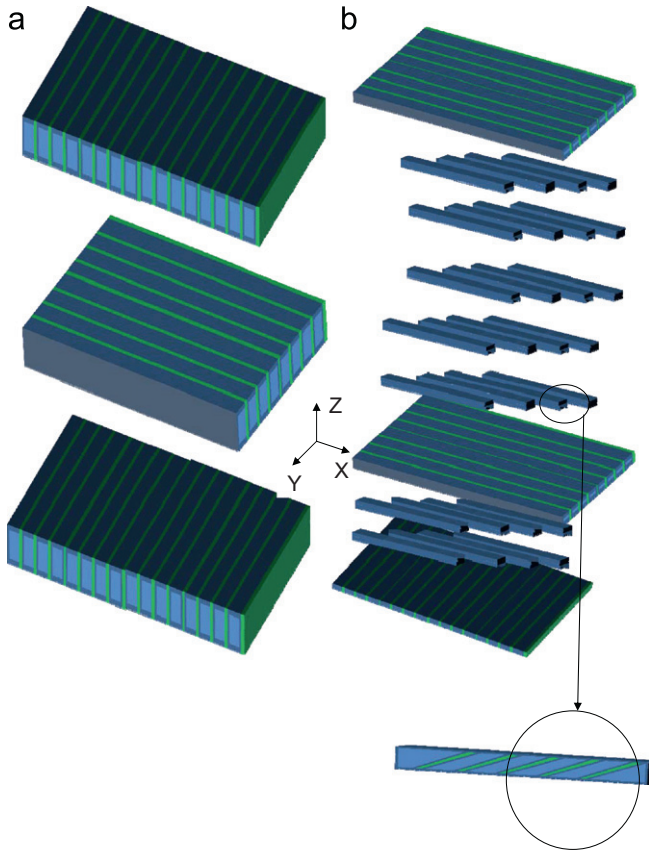

Fig. 6. Design prototypes (a) SG-A and (b) SG-B.

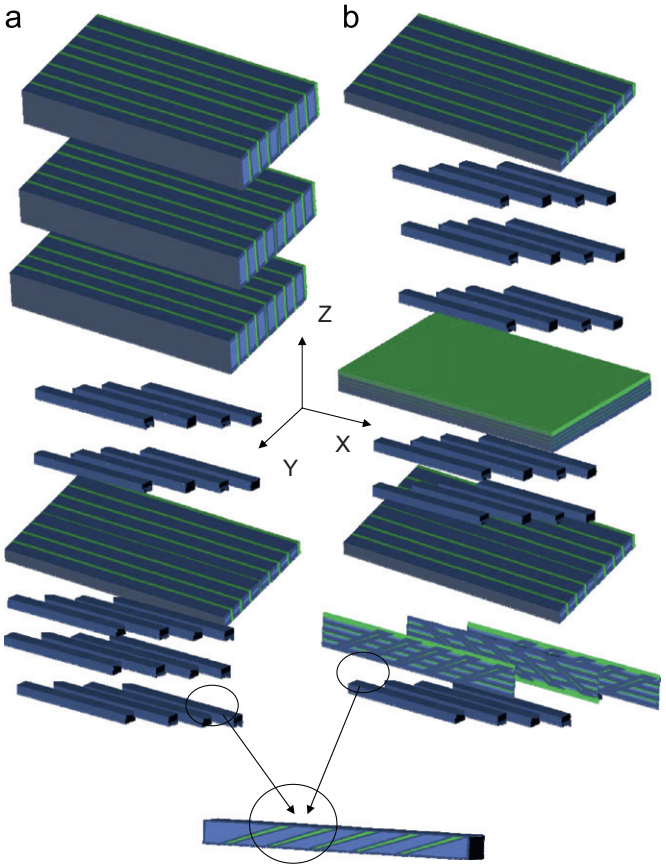

Fig. 7. Design prototypes (a) SG-C and (b) SG-D.

SG-B (Fig. 6b) sought to increase the layer complexity/density by going from three macrolayers in SG-A to ten macrolayers. The bottom-most macrolayer in SG-B (Fig. 6b) or macrolayer 1, is a tunnel-cracking *YZ* layer (Fig. 3). Macrolayers 2, 3, and 5–9 have a second-order structure. Each of these macrolayers is comprised of multiple parallel first order laths, each of which has multiple parallel second order laths orientated at $\pm 45^{\circ}$ to the long axis of their first order laths (lamellae). Adjacent first order laths in such a macrolayer have the second order lamellae (laths) that are perpendicular in orientation. In addition, the first order laths in these macrolayers were made with small widths (0.6 mm) to accommodate a total of more than six such laths, across the width of a 4 mm wide bend-test bar. A thin coating of BN was applied between the ten macrolayers of SG-B with the goal of providing additional delamination paths for fracture. The fourth and tenth macrolayers had the *XZ* configuration (Fig. 3) to provide additional strength and stiffness near the neutral axis and the compressive surface of the bend specimens. *XZ* macrolayers do not provide natural, easy pathways for cracks to propagate in the four-point bend test.

In SG-C (Fig. 7a), the tunnel cracking first-order layer was eliminated, and a more liberal coating of BN was used between layers to encourage crack deflection and arrest. SG-C had only two kind of macrolayers; those with the second order structures and others with the *XZ* architecture. The objective was to combine the toughness from the second-order macrolayers and the strength from the *XZ* macrolayers. SG-C had a total of nine macrolayers. In SG-D (Fig. 7b), a strong *XY* layer was added at the neutral axis of the bend specimens, and more importantly a layer with a third order structure was introduced as the second macrolayer from the bottom. SG-D was the only design prototype with a third order structure in a macrolayer.

4. Characterization of biomimetic ceramics

The mechanical properties of the biomimetic SG ceramics were determined with the focus on the ability of these ceramics to withstand applied mechanical loads. A principal property determined was the work-of-fracture (WOF). Work-of-fracture is a convenient metric for assessing the ability of ceramics to resist catastrophic fracture [25]. It is usually determined by conducting a quasi-static four-point bend test on a standardized test specimen geometry. The test specimen was a rectangular bar with a cross section of 4 mm × 3 mm. The outer loading span was 40 mm and the inner loading span 20 mm. All surfaces of the specimens were ground with a 400 grit diamond grinding wheel and the tensile surface of each specimen was further polished to a 1 μm diamond finish. The test specimen was placed in the four-point-bend fixture and loaded in a testing machine. Loading was performed in a servohydraulic machine (MTS 810, MTS Systems Corporation, Eden Prairie, MN) under displacement control with a crosshead speed of 0.05 mm/min. The load vs. crosshead displacement was recorded. The area under the load-displacement curve is a measure of the work performed to cause complete failure of the specimen. This area (work) is divided by twice the cross section area of the rectangular cross section to establish the work-of-fracture (WOF) of the specimen. The work-of-fracture is not an intrinsic property of a material. It is dependent on the test method, specimen size, and shape. It is still a very useful metric for comparing the ability of various ceramics to resist catastrophic fracture. Some bending tests were performed on bend test samples that were indented. These indents were made with a Macro Vickers hardness tester (LECO LV-100, LECO Corporation, St. Joseph, MI).

Specimens for microstructure characterization were polished down to 1 μm diamond. Imaging was done using an optical microscope as well as a Field Emission Scanning Electron Microscope (Hitachi S-4800-1, Hitachi HTA, Pleasanton, CA). Fracture surfaces were directly observed in the Scanning Electron Microscope.

5. Results and discussion

5.1. Microstructure

The processing techniques developed in our work have been successful at fabricating hierarchical structures. This is evidenced by the structures seen in Fig. 8, from an early design prototype. Rectangular cells which represent cross sections of the first order laths are clearly visible in Fig. 8. These resemble the structure of the Strombus gigas as shown in Kamat et al. [14]. These rectangular cellular first order regions are also visible in the lower half of the cross sectional view of an SG-C four-point bend bar specimen (see Fig. 9). These cells have a characteristic width on the order of 0.6 mm. Also visible within each of the first order

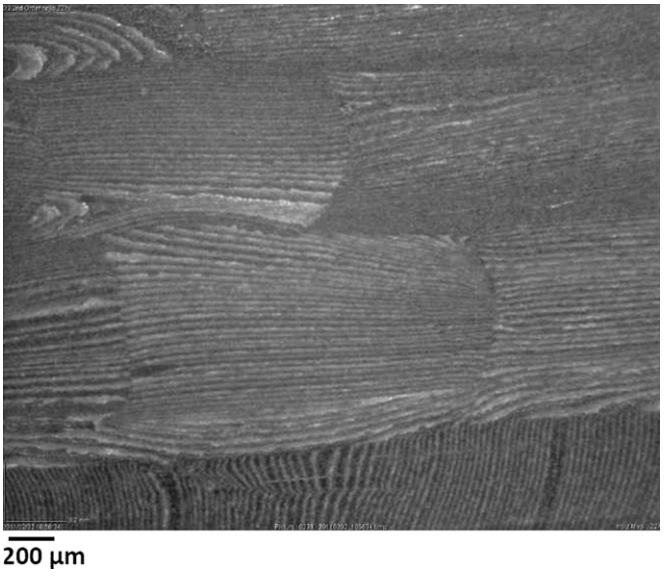

Fig. 8. The cross sectional view of a biomimetic SG ceramic four-point bend bar specimen. The first order and second order structures are visible in the micrograph.

Fig. 9. Optical cross section view of an SG-B four-point bend bar specimen. Cross section was obtained by an inclined cut at 60°. Rectangular cells representing cross section views of the first order lamellae are seen in this cross section. Also visible are the second order layers within each rectangular first order cell.

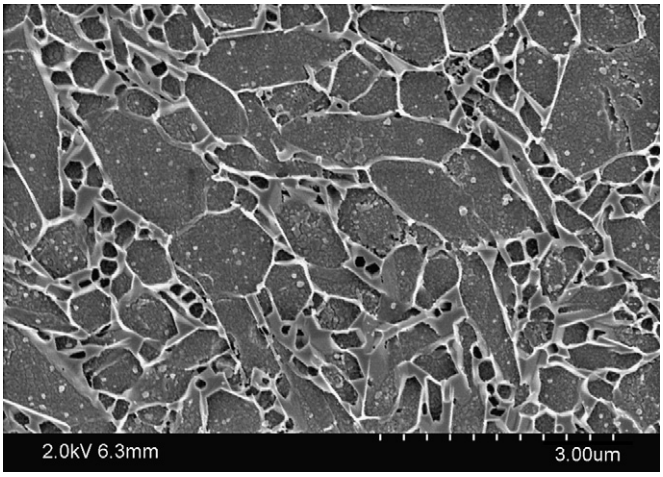

Fig. 10. Silicon nitride grains in a layer of silicon nitride in a second order region of SG-B.

rectangular cells (Figs. 8 and 9) are the cross section views of the second order lamellae. The orientations of the second order lamellae are not obvious in these views but would be at $\pm 23^\circ$, $\pm 23^\circ$, and $\pm 16^\circ$ to the long axis of the first order lamellae for SG-B, SG-C, and SG-D, respectively. Second order structures seen in Figs. 8 and 9 have a characteristic dimension of the order of 10−20 μm. Within each thin layer of silicon nitride, irrespective of the order of the structure, silicon nitride grains are formed. Fig. 10 shows silicon nitride grains in a region of silicon nitride with a second order structure.

5.2. Mechanical properties

Table 1 reports the WOF values of several biomimetic architectures SG-A, SG-B, SG-C, and SG-D. Representative load vs. displacement plots that lead to the calculation of the work-of-fracture for these architectures are shown in Fig. 11. A more nuanced look at the work-of-fracture (WOF) involves looking at it as the sum of two components: a pre-peak WOF and a post-peak WOF. The pre-peak WOF is a measure of the elastic energy stored in the material just prior to crack initiation. The post-peak WOF is a measure of the ability of the material to continue to provide load-bearing capability even after a crack has been initiated in it at the peak load. Table 1 shows a breakdown of the WOF into pre-peak and post-peak components for our design architectures. The results reported are for sample sizes of three. The total WOFs represent the area under the load displacement graphs divided by twice the cross section area of the bend test specimens. The pre-peak WOFs are obtained using the area under the load-displacement graphs to the left of the peak load value. The post-peak WOFs utilize the area under the graphs from the peak load value until final fracture.

The results shown here suggest that SG-D is the best performing biomimetic sample with the highest total WOF. SG-D is also the best performing sample when it comes to graceful failure, or non-catastrophic failure since it has the highest post-peak WOF. In addition to the average values shown here, it is also important to note the highest performing tests. In highlighting the best performing tests from each of the samples (Table 2), a clearer idea is obtained on which designs have the highest potential.

The total WOFs of the biomimetic ceramics in Tables 1 and 2 compare very favorably with WOF results reported for Fibrous Monolith Si_3N_4-BN ceramics in the literature [26,27,22]. Koh et al. [27] report a WOF of 1216 J/m^2 for an FM silicon nitride/boron nitride material system. Zok et al. [26] tested two different architectures of silicon nitride/boron nitride FMs; the 0°/90° and the +45°/−45°. Their measured WOFs for the two architectures were 2700 J/m^2 and 5600 J/m^2, respectively. Fig. 12 shows a load vs. displacement plot from a four point bend test of a 0°/90° silicon nitride/boron nitride FM reported in Kovar et al. [23]. The total WOF for the FM of Fig. 12 is 2860 J/m^2, with a post-peak WOF of 1050 J/m^2. Clearly the SG-D biomimetic architecture performs very favorably in comparison with the 0°/90° FM architecture.

A particularly desirable trait that sea-shells like Strombus gigas possess is damage tolerance. Their ability to sustain damage inflicted by nature or by predators and yet retain a substantial fraction of their original strength is well known. The damage tolerance of the biomimetic ceramics is assessed by indenting four point bend specimens in a Macro Vickers hardness tester. The load used to create the indent is 50 kg with an indentation dwell time of 15 s. Typical indents and the damage surrounding them in SG-C and SG-D specimens are shown in Fig. 13. The response of an undamaged and a damaged bend test specimen in a four point bend test is compared by constructing a metric called the DT-50 metric. The DT-50 metric is the ratio of the work-of-fracture of specimens indented by a 50 kg load and that of nominally

identical but unindented specimens. This DT-50 WOF metric is reported for a monolithic silicon nitride specimen and two biomimetic SG Si_3N_4-BN ceramics, SG-C and SG-D, in Table 3. For both SG-C and SG-D, the DT-50 WOF metric is close to 1.0, which is indicative of the fact that the WOF magnitude of these materials is relatively unaffected by the presence of a large defect caused by a fairly severe indentation load of 50 kg. This is a demonstration of their damage tolerance. A monolithic silicon nitride on the other hand is severely impacted by such an indentation and shows a very steep drop in its WOF (Table 3). The metrics in Table 3 are constructed using the average values of WOF for sample sizes of three.

Several toughening mechanisms seen in Strombus gigas shells are observed in the biomimetic ceramics. Tunnel cracking, seen in the first order interfaces of the inner and outer layers of the sea shell are seen in the first order interfaces of the outermost (tensile) layer of a SG-B specimen in four point bending (Fig. 14). A second mechanism is crack bridging as seen in Fig. 15, in a biomimetic SG-B.

In addition, we observed signs of fiber like sliding. The complex structure of Strombus gigas also causes tortuous

Table 1
Average pre-peak, post-peak, and total WOF values for biomimetic designs.

Biomimetic designs	Pre-peak WOF (J/m^2)	Post-peak WOF (J/m^2)	Total WOF (J/m^2)
SG-A	230	70	300 ± 21
SG-B	360	500	860 ± 120
SG-C	810	750	1560 ± 240
SG-D	1320	910	2230 ± 920

Table 2
Largest post-peak, and total WOF values for biomimetic designs.

Biomimetic designs	Post-peak WOF (J/m^2)	Total WOF (J/m^2)
SG-A	110	320
SG-B	500	850
SG-C	1000	1800
SG-D	1340	3620

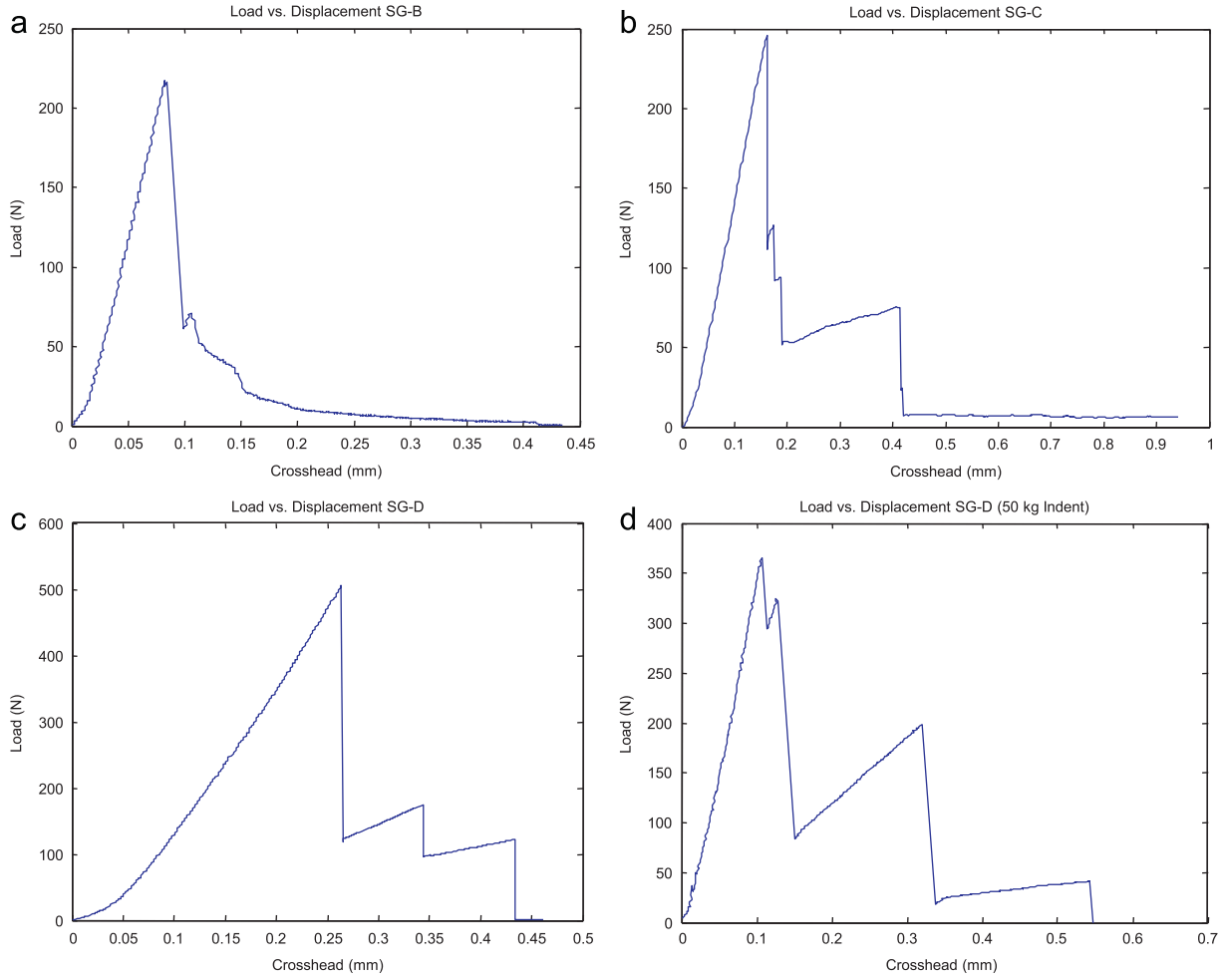

Fig. 11. Four point bend test load vs. displacement for biomimetic ceramics; (a) SG-B, (b) SG-C, (c) SG-D, and (d) indented SG-D specimen.

crack paths and crack deflection, thus providing another mechanism for toughening. These tortuous paths are apparent in Fig. 16 from a variety of biomimetic designs. Thus, all the toughening mechanisms seen in the Strombus gigas shell have been reproduced in the biomimetic ceramics.

6. Conclusions

SHELL has proven to be very effective in constructing biomimetic SG ceramics (in bulk form 25 mm × 75 mm × 4 mm) whose architecture mimics the crossed lamellar structure of the Strombus gigas shell. The smallest feature size achieved is 1 μm. First, second, and third order structures have been built in the biomimetic SG ceramics that resemble the Strombus gigas in geometry, although the scale of the second and third order structures in the biomimetic SG ceramics is larger.

The ability of the biomimetic SG ceramics to absorb energy during fracture was assessed by determining the work-of-fracture in four point bending tests. Quantitative assessment of damage tolerance was performed by experimentally

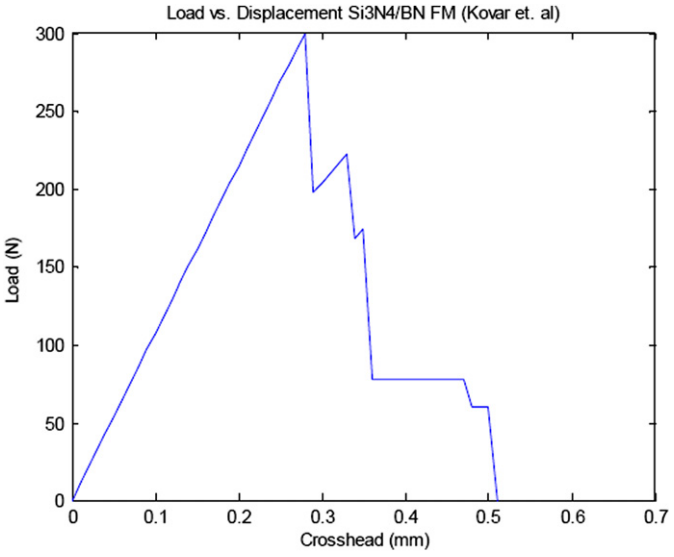

Fig. 12. Four point bend test load vs. displacement for a Fibrous Monolith SiN/BN adapted from [23].

Table 3
DT-50 WOF metric for the biomimetic SG-C and SG-D compared with a monolithic silicon nitride.

Material	Monolithic silicon nitride	SG-C	SG-D
DT-50 WOF metric	0.095	0.83	0.79

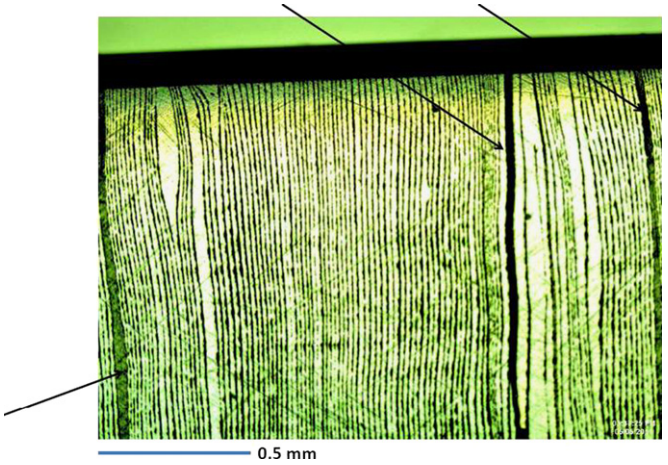

Fig. 14. Tunnel cracks in the first order interfaces of a SG-B ceramic. Tunnel cracks are indicated by the bold arrows.

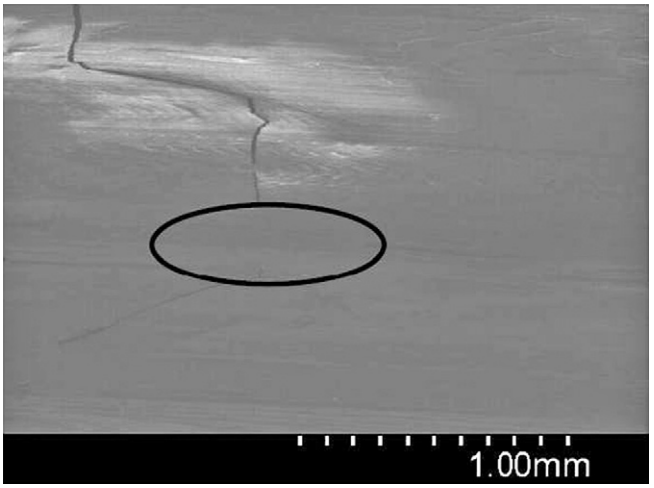

Fig. 15. Crack bridging observed in biomimetic ceramic SG-B.

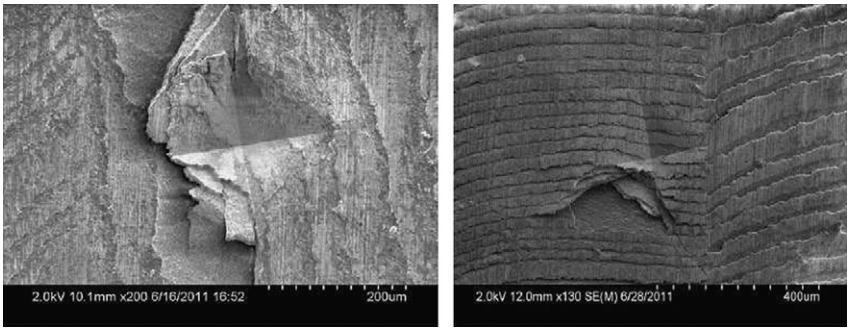

Fig. 13. Indents created by a Macro Vickers hardness indent under a 50 kg load. (Left) SG-C and (right) SG-D.

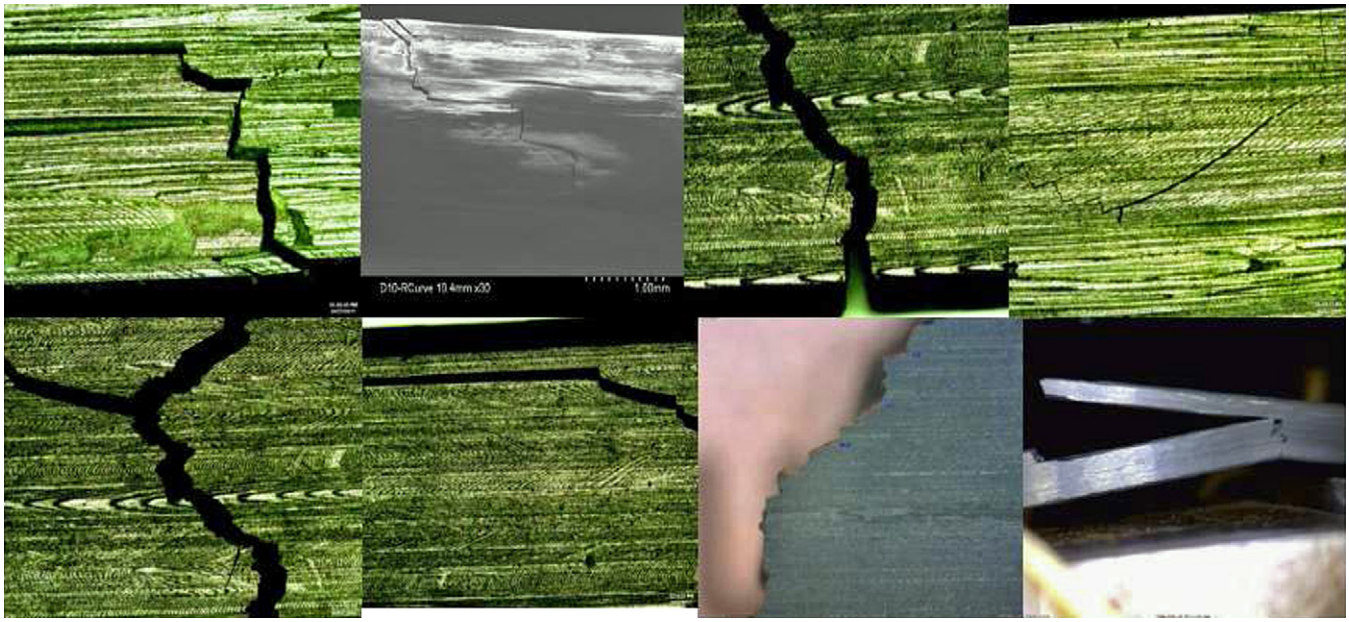

Fig. 16. Fracture paths in several biomimetic ceramic architectures.

quantifying the total WOF, the post-peak WOF, and by evaluating the DT-50 metric, which is a measure how an indented (damaged) specimen behaves in comparison to undamaged specimens. The post-peak WOF and the damage tolerance metric (DT-50) of design prototype SG-D are very promising. The post-peak WOF of SG-D is 1.5× the post-peak WOF of a baseline Fibrous Monolith silicon nitride material. The damage tolerance of SG-D is in particular very encouraging as the material seems to be almost immune to damage caused by a quasi-static indentation of 50 kg. Its damage tolerance far exceeds that of a monolithic silicon nitride.

We speculate that SHELL can be used to process other material systems including ceramic-metal or ceramic-organic systems. In addition, it is anticipated that quantitative performance gains may be achieved in future biomimetic SG ceramics by increasing the complexity of the designs, minimizing the distortions in the builds, and incorporating nano-sized powders to provide reductions in the second and third order scales. SHELL processed ceramics may offer a superior alternative to Ceramic-Matrix-Composites or armor materials as their hierarchical structures are optimized. In addition, SHELL offers a route to tailor the electromagnetic properties of advanced ceramics by adjusting the feature length scales to match the wavelength of incident radiation.

Acknowledgments

The National Science Foundation supported this research through an STTR Phase I award (IIP-1010312). A Major Research Instrumentation award (Award Number 0521011) from the National Science Foundation enabled the imaging of the microstructures using the high resolution scanning electron microscope.

References

[1] C. Ortiz, M. Boyce, Bioinspired structural materials, Science 319 (2008) 1053–1054.
[2] P. Fratzl, Biomimetic materials research: what can we really learn from nature's structural materials?, Journal of the Royal Society Interface 4 (2007) 637–642.
[3] G.M. Luz, J.F. Mano, Biomimetic design of materials and biomaterials inspired by the structure of nacre, Philosophical Transactions of the Royal Society A 367 (2009) 1587–1605.
[4] J.D. Currey, The design of mineralized hard tissues for their mechanical functions, Journal of Experimental Biology 202 (1999) 3285–3294.
[5] F. Berthelat, Biomimetics for next generation materials, Philosophical Transactions of the Royal Society A 365 (2007) 2907–2917.
[6] R.Z. Wang, Z. Suo, A.G. Evans, N. Yao, I.A. Aksay, Deformation mechanisms in nacre, Journal of Materials Research 16 (9) (2001) 2485–2493.
[7] H.D. Espinosa, J.E. Rim, F. Berthelat, M.J. Buehler, Merger of structure and material in nacre and bone—perspectives on de novo biomimetic materials, Progress in Materials Science 54 (2009) 1059–1100.
[8] K.S. Katti, D.R. Katti, Why is nacre so tough and strong?, Materials Science and Engineering C 26 (2006) 1317–1324.
[9] X. Li, W.C. Chang, Y.J. Chao, R. Wang, M. Chang, Nanoscale structural and mechanical characterization of a natural nanocomposite material: the shell of red abalone, Nano Letters 4 (4) (2004) 613–617.
[10] D.F. Hou, G.S. Zhou, M. Zheng, Conch shell structure and its effects on mechanical behaviors, Biomaterials 25 (2004) 751–756.
[11] S. Kamat, H. Kessler, R. Ballarini, M. Nassirou, A.H. Heuer, Fracture mechanisms of the Strombus gigas conch shell: II—micromechanics analyses of multiple cracking and large-scale crack bridging, Acta Materialia 52 (2004) 2395–2406.
[12] N.M. Neves, J.F. Mano, Structural/mechanical behavior relationships in crossed-lamellar seashells, Materials Science and Engineering C 25 (2005) 113–118.
[13] M.A. Meyers, A.Y.M. Lin, Y. Seki, P.Y. Chen, B.K. Kad, S. Bodde, Structural biological composites: an overview, Journal of Materials (July) (2006) 35–41.

[14] S. Kamat, X. Su, R. Ballarini, A.H. Heuer, Structural basis for the fracture toughness of the shell of the conch Strombus gigas, Nature 405 (2000) 1036–1040.
[15] W.J. Clegg, K. Kendall, N.M. Alford, T.W. Button, J.W. Birchall, A simple way to make tough ceramics, Nature 347 (1990) 455–457.
[16] G. Mayer, New classes of tough composite materials: lessons from natural rigid biological systems, Materials Science and Engineering C 26 (8) (2006) 1261–1268.
[17] M.E. Launey, E. Munch, D.H. Alsem, E. Saiz, A.P. Tomsia, R.O. Ritchie, A novel biomimetic approach to the design of high performance ceramic metal composites, Journal of the Royal Society Interface 7 (2010) 741–753.
[18] Z.Y. Tang, N.A. Kotov, S. Magonov, B. Ozturk, Nanostructured artificial nacre, Nature Materials 2 (6) (2003) 413–418.
[19] L. Chen, R. Ballarini, H. Kahn, A.H. Heuer, Bioinspired micro-composite structure, Journal of Materials Research 22 (1) (2007) 124–131.
[20] V.S. Kaul, K.T. Faber, Synthetic crossed lamellar microstructures in oxide ceramics, Journal of Ceramic Processing Research 6 (3) (2005) 218–222.
[21] W. Coblenz, Fibrous monolithic ceramic and method for production, US Patent 4,772,524 (1988).
[22] S. Baskaran, S.D. Nunn, D. Popovic, J.W. Halloran, Fibrous monolith ceramics: I, fabrication, microstructure, and indentation behavior, Journal of the American Ceramic Society 9 (1993) 2209–2216.
[23] D. Kovar, B.H. King, R.W. Trice, J.W. Halloran, Fibrous monolithic ceramics, Journal of the American Ceramic Society 80 (10) (1997) 2471–2487.
[24] S. Baskaran, S.D. Nunn, J.W. Halloran, Fibrous monolithic ceramics: IV, mechanical properties and oxidation behavior of the alumina/nickel system, Journal of the American Ceramic Society 77 (5) (1994) 1256–1262.
[25] R.W. Trice, J.W. Halloran, Elevated temperature mechanical properties of silicon nitride/boron nitride fibrous monolithic ceramics, Journal of the American Ceramic Society 83 (2) (2000) 311–316.
[26] J.C. McNulty, M.R. Begley, F.W. Zok, In-plane fracture resistance of a cross-ply fibrous monolith, Journal of the American Ceramic Society 84 (2) (2001) 367–375.
[27] Y.H. Koh, H.W. Kim, H.E. Kim, Mechanical properties of fibrous monolithic silicon nitride/ boron nitride ceramics with different cell boundary thicknesses, Journal of the European Ceramic Society 24 (2004) 699–703.